Applied Surface Science 542 (2021) 148556

Contents lists available at ScienceDirect

Applied Surface Science

journal homepage: www.elsevier.com/locate/apsusc

Full Length Article

# N-doping enabled defect-engineering of $MoS_2$ for enhanced and selective adsorption of $CO_2$: A DFT approach

Francis M. Enujekwu [a,b,1], Yue Zhang [c], Collins I. Ezeh [a], Haitao Zhao [d], Mengxia Xu [a,b], Elena Besley [e], Michael W. George [a,e], Nicholas A. Besley [e], Hainam Do [a,b], Tao Wu [a,b,*]

[a] Department of Chemical and Environmental Engineering, The University of Nottingham Ningbo China, Ningbo 315100, China
[b] Key Laboratory for Carbonaceous Waste Processing and Process Intensification Research of Zhejiang Province, The University of Nottingham Ningbo China, Ningbo 315100, China
[c] Department of Civil Engineering, Qingdao University of Technology, 266033 Qingdao, China
[d] Department of Mechanical Engineering, Massachusetts Institute of Technology, Cambridge, MA 02139, United States
[e] School of Chemistry, The University of Nottingham, University Park, Nottingham NG7 2RD, UK

ARTICLE INFO

*Keywords:*
Carbon dioxide
Molybdenum disulfide
Carbon capture
Density functional theory
Computational analysis

ABSTRACT

A density functional theory study was conducted to analyze $CO_2$ adsorption on defective and non-defective $MoS_2$ surfaces with or without nitrogen doping. The $MoS_2\_1V_S$ and $MoS_2\_1V_{Mo}\_3N_S$ were found exhibiting outstanding adsorption activity and stability, which is linked to an enhanced electron charge on the surface in the presence of vacancies and N species that alters strength and type of interactions with $CO_2$ molecules. Results showed the dissociative chemisorption of $CO_2$ on the $MoS_2\_1V_s$ and a significantly enhanced physisorption of $CO_2$ on the $MoS_2\_1V_{Mo}\_3N_S$, which displays an adsorption energy of −1.818 eV compared with −0.139 eV of the pristine $MoS_2$ surface. Meanwhile, the $MoS_2$_1Vs exhibits an excellent selective adsorption of $CO_2$ over $N_2$ and $H_2O$, with the highest adsorption ratio of 5.1 and 3.5, respectively. Partial dissociation of $CO_2$ to CO over the $MoS_2$_1Vs is also observed and attributed to increased covalent attractions at the vacant site, while the improved $CO_2$ physisorption over the $MoS_2\_1V_{Mo}\_3N_S$ is attributed to the enhanced electrostatic interactions at the vacancy site due to N doping. These findings are confirmed by the computed vibrational frequencies of $CO_2$ bound on these surfaces. The N-doping enabled defect engineering of $MoS_2$ is proved effective and enhanced selective adsorption of $CO_2$.

## 1. Introduction

$CO_2$ capture is essential to mitigate global climate change caused by anthropogenic $CO_2$ emission [1]. Existing $CO_2$ capture technologies exhibit a high range of cost estimates, which depends on process type, separation technology, $CO_2$ transport technique and storage site [2]. Hence, research is needed to develop highly effective capture materials that can overcome the cost implications of existing technologies.

Monolayer molybdenum disulphide ($MoS_2$) is one of the two-dimensional (2D) transition-metal dichalcogenides (TMD) that have been the focus of considerable interest over the past two decades [3] due to much success in applications in electronics, energy storage, sensing, and photoluminescence [4]. As in the well-studied cases of graphene and graphene oxide (GO) [5–9], the high surface to volume ratio of mono and few layers TMD can be exploited for gas sensing applications. Detection of $CO_2$ using highly reduced GO flakes has been shown to be effective as the low adsorption strength of $CO_2$ on GO flakes surface results in easy desorption of gas molecules without light assistance [10]. Unlike graphene which has a zero band gap, $MoS_2$ is a semiconductor with a band gap ranging from 1.2 eV (indirect) in bulk [11] to 1.9 eV (direct) in monolayer [12]. This change in band gap gives rise to the novel photoluminescence and electronic properties of the $MoS_2$ monolayer and might unlock the potential of this material as gas sensor and as an alternative material for $CO_2$ capture.

Calculations based on density functional theory (DFT), show that pollutant gases such as $NO_2$, NO and $SO_2$, can strongly interact with $MoS_2$ surfaces owing to the charge transfer mechanism between gas molecules and $MoS_2$, which explains its gas sensing properties [13,14].

* Corresponding author at: Department of Chemical and Environmental Engineering, The University of Nottingham Ningbo China, Ningbo 315100, China.
*E-mail address:* tao.wu@nottingham.edu.cn (T. Wu).
[1] F.M.E. and Y.Z. contributed equally.

https://doi.org/10.1016/j.apsusc.2020.148556
Received 11 July 2020; Received in revised form 13 November 2020; Accepted 19 November 2020
Available online 2 December 2020

DFT calculations also show that $MoS_2$ adsorbs $H_2$ molecules, which prefer to bind with the S atoms of the monolayer thus enhancing its conductivity [15]. For non-polar gas molecules, like $CO_2$ and $CH_4$, the perfect $MoS_2$ surface cannot offer strong adsorbing sites, and the presence of defects, especially S vacancies, is essential to result in the possibility for these molecules to adsorb on $MoS_2$ [16]. Another important feature is the large surface area created when the bulk is thinned into layers, with the surface area of exfoliated $MoS_2$ flakes having a high density of edges which are potential active sites for electrochemical applications in sensing and energy storage, in particular for $CO_2$ storage [3,4]. As the edge sites of $MoS_2$ flakes are more reactive than the surface, orientation of the flakes can be used to tune their response to target specific gases.

To date, numerous strategies have been employed for the fine-tuning of the physical and chemical properties of $MoS_2$ and other TMD materials [11,17–19]. Both experimental and theoretical studies have been used to investigate point defects in the $MoS_2$ monolayer [20,21]. These studies have revealed that point defects are usually more reactive than the sites present on a perfect surface. The single sulfur vacancy (S-vacancy) point defect is more easily formed than anti-site defects [20] and the edge is usually less stable and more prone to doping [22]. The results showed that the defective $MoS_2$ surface improved the adsorption strength and catalytic activity of the $MoS_2$ layer [21,22].

An alternative way to improve $CO_2$ uptake capacity is to create basic or redox-active surface sites by incorporating nitrogen into the surface framework, which manipulates its conductivity and charge density [11,23,24]. This promotes the transfer of electrons between the surface and $CO_2$, therefore enhancing the energy storage activities [25]. A recent DFT study proposed that nitrogen doping in monolayer $MoS_2$ leads to a high electronic state density around the N and Mo atoms and therefore enhancing its electronic conductivity [11]. The synergistic effect of molecular doping and vacancy defects may further enhance the $CO_2$ adsorption activity of $MoS_2$. However, despite the numerous investigations on molecules interacting with pristine [26,27] and defective [21,22] monolayer $MoS_2$, there has not been an extensive study on $CO_2$ adsorption on N atom doped $MoS_2$, which has the potential to pave the way towards developing an engineered $MoS_2$ nanosheets with sufficient active sites for enhanced $CO_2$ adsorption capacity.

In this study, we present a fundamental understanding of exploiting nitrogen doping (N-doping) for the preparation of defect-rich $MoS_2$ with enhanced $CO_2$ adsorption capacity is. The first-principles DFT study was carried out to investigate $CO_2$ adsorption on defect-free monolayer $MoS_2$ as well as $MoS_2$ surface with different types of vacancies (single and double vacancies) with and without N-doping. The influence of different

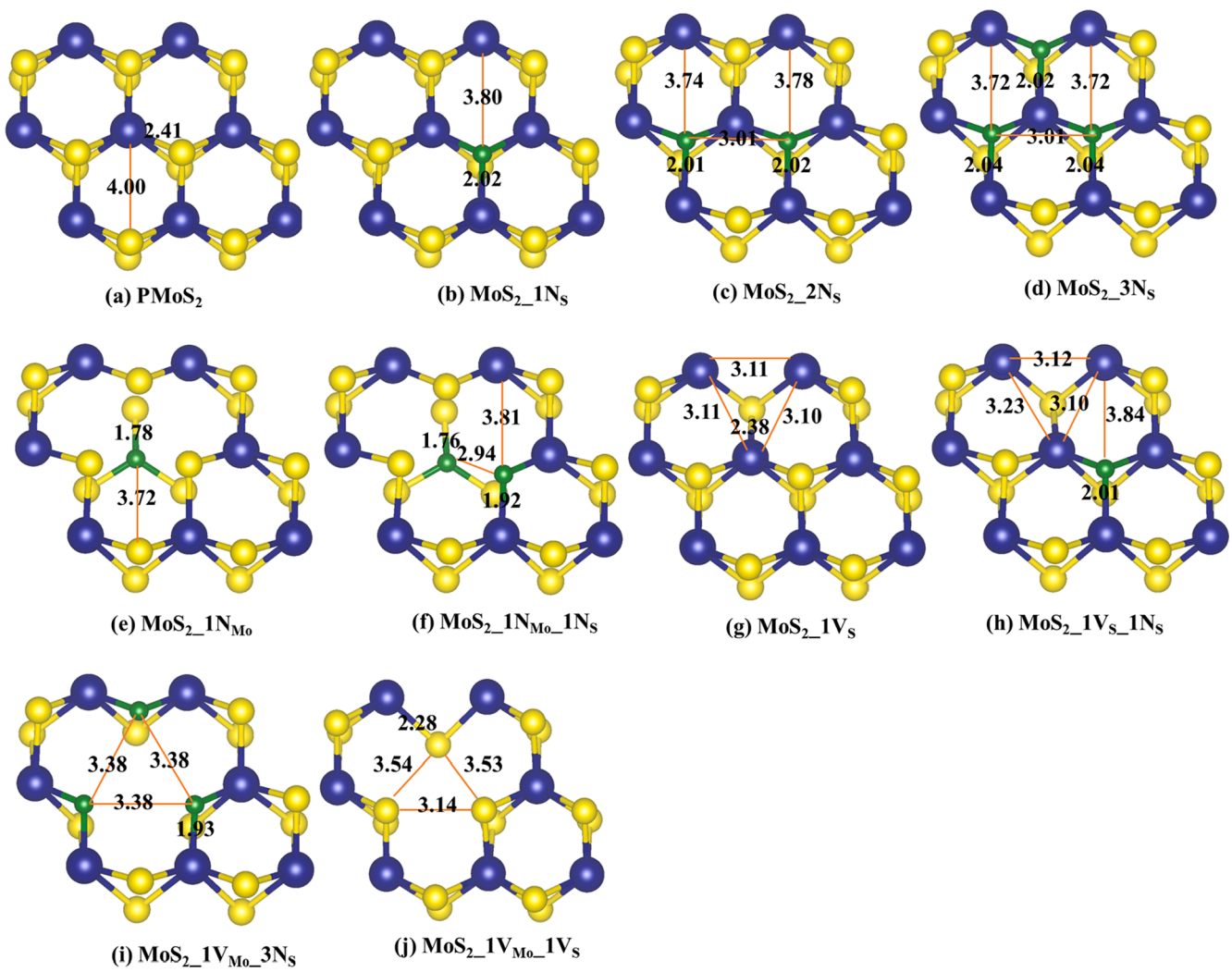


**Fig. 1.** Relaxed local geometric configurations of $MoS_2$ (a) pristine (b) one S atom substituted with a N atom (c) two S atoms substituted with two N atoms (d) three S atoms substituted with three N atoms (e) one Mo atom substituted with one N atom (f) Mo and S atoms substituted with two N atoms (g) $MoS_2$ with 1 S-vacancy (h) one S atom substituted with one N atom in $MoS_2$ with 1 S-vacancy (i) three neighboring S atoms in a unit cell substituted with three N atoms in 1 Mo-vacancy defect and (j) 1Mo and 1S vacancy-defected $MoS_2$. Color code: Mo, blue, S, yellow, and N, green. The lines define the lengths given in Å. (For interpretation of the references to colour in this figure legend, the reader is referred to the web version of this article.)

types of vacancies and level of N-doping on the structural and electronic properties of the $MoS_2$ monolayer was investigated. In addition, how N-doping and various types of vacancies govern the electron transfer rate as well as the efficacy for $CO_2$ adsorption were explored. Infrared (IR) spectroscopy was also performed to probe the structure of the surface adsorbates. The adsorption of nitrogen and water molecules was investigated to ascertain the selective adsorption of $CO_2$.

## 2. Computational methods

A periodic (4 × 4 × 1) supercell of the $MoS_2$ monolayer ($PMoS_2$) containing 48 atoms (16 Mo atoms and 32 S atoms) is used as an initial computational model. The lateral value of the box is 12.76 Å × 12.76 Å [28]. A large vacuum layer of 15 Å in the direction to the interface is used as an isolated slab boundary condition to avoid interlayer interactions. The positions of all the atoms in the supercell were fully relaxed during structural optimization for all the supercells with or without defects. In order to simulate the vacancy defect $MoS_2$ systems, one or two adjacent Mo or S atoms were removed to create a stable single or double vacancy-defected $MoS_2$ (Fig. 1) consistent with the literature [29]. Also, Mo or S atoms were substituted with N atom (s) to simulate N-doped $MoS_2$ defect complex systems as shown in Fig. 1. Additional details can be found in the Supporting Information Section 1 and Section 2.

The simulations use spin-polarized DFT-D2 calculations using Grimme's [30] method, as implemented in Vienna *ab initio* simulation package (VASP) [31,32]. This approach adds a semi-empirical pairwise force field to the conventional first-principles plane-wave DFT calculations. This takes dispersion interactions into consideration, and it accurately describes the interactions for adsorption systems [33]. The exchange-correlation potential is treated with the generalized gradient approximation (GGA) functional of Perdew, Burke and Ernzerhof (PBE) [34]. A 500 eV cutoff energy was used for the plane-wave basis set. Γ-center meshes of 5x5x1 and 9x9x1 Monkhorst-Pack [35] k-point are used for sampling the Brillouin zone during geometry optimization and density of state calculations, respectively. The Gaussian smearing width was set to 0.2 eV. For geometry relaxation, we used the method of conjugate gradient energy minimization with convergence criterion for the energy of $10^{-6}$ eV between two consecutive steps, and the maximum Hellmann-Feynman force exerting on each atom less than 0.01 eV/Å upon ionic relaxation. In order to test for cutoff energy and k-point grid is required convergence, two denser Monkhorst-Pack grids (6x6x1 and 7x7x1) and a cutoff energy (600 and 700 eV) were tested for all the simulated systems. The results were compared for several selected parameters. It was found that the results from 5x5x1 Monkhorst-Pack grids were very similar to those for the 6x6x1 and 7x7x1 Monkhorst-Pack grids. The total energy was converged to <10 meV. Hence, we believe that 5x5x1 Monkhorst-Pack is dense enough for 4x4x1 $MoS_2$ monolayer and that 500 eV cutoff energy is suitable for the plane-wave basis set. Using Bader charge analysis, charge transfer between molecules and the substrate is obtained [36]. All calculations are performed under the same relaxation criteria.

The frequencies of the phonon modes for the physiosorbed and dissociated state have been calculated through finite difference method using a displacement of 0.015, and by fixing all of the atoms of the $MoS_2$ monolayer. This approach has shown to introduce little or no error in the computed frequencies and intensities of the adsorbed molecules and results in significant reduction in computational cost [37]. The vibrational modes of the molecules in gas phase were also computed to compare with the different adsorption configurations.

The binding energy of the N atom(s) on $MoS_2$ surface, $E_{bN}$, isosurfaces of the spin charge density difference for the defective $MoS_2$ monolayer, $\Delta\rho_s$, adsorption energy ($E_{AE}$), charge density difference of the adsorption systems, $\Delta\rho_{df}$, were calculated using Equations (S1-S3), (S4), (S5) and (S6), respectively, as described in Supporting Information (S1.3).

## 3. Results and discussion

In total, 10 possible surface configurations consisting of non-defective and defective periodic (4 × 4 × 1) supercell of the $MoS_2$ monolayer were investigated (see Fig. 1). The corresponding stable localized configurations for N doping and vacancies are shown in Fig. 1. The formation of these configurations are detailed in the Supporting Information (Section S1.2).

### 3.1. Properties of N-doped defective and non-defective $MoS_2$ monolayer

Prior to evaluating the adsorption of $CO_2$, the relative properties (atomic, electronic and magnetic) of the simulated surface configurations are discussed. To reveal the effects of N atoms and vacancy defects on the structural properties of the adsorbent, the results of the N substitutional and N-doped vacancy (Mo and S) defect systems are compared with that of the optimized $MoS_2$ monolayer. The results of the structural geometry of the optimized $MoS_2$ monolayer is presented in the Supporting Information (Table S1), which agrees well with the experimental data [38] and previous theoretical values [26,39]. The simulation results of the single ($MoS_2\_1V_S$) and double vacancy ($MoS_2\_1V_{Mo}\_1V_S$) defect systems are presented in the Supporting Information (Table S2). The results agree well with previous studies [28,29]. The binding energy of N atom(s) on $MoS_2$ surface, $E_{bN}$, was calculated using Equations (S1-S3) as described in Supporting Information (S1.3).

Table 1 presents the binding energy and bond length of N-doped monolayer $MoS_2$ at different sites using the DFT calculations illustrated in Fig. 1. The binding energies of all N-doped $MoS_2$ surfaces are negative (exothermic process), which suggests that it is viable for N atoms to be filled into the $MoS_2$ surfaces. Among the N-doped $MoS_2$ monolayers, the $MoS_2\_1N_{Mo}\_1N_S$ displayed the highest binding energy of −11.49 eV upon optimization. Similarly, the $MoS_2\_1N_{Mo}$ showed a relatively high binding energy (−8.07 eV), but lower than that of $MoS_2\_1N_{Mo}\_1N_S$ due

**Table 1**
Summary of N-doped $MoS_2$ configurations.

| Model | $E_{bN}$, eV | $E_g$[a], eV | $Q_N$[b], e | $M_N$[c], $\mu_B$ | $d_{Mo-S}$[d], Å | $d_{N-Mo}$[e], Å | $h_{N-S}$[f], Å |
|---|---|---|---|---|---|---|---|
| $MoS_2\_1N_S$ | −0.88 | 1.71 | −0.81 | 0.23 (0.83) | 2.45 | 2.02 | 2.69 |
| $MoS_2\_2N_S$ | −1.63 | 1.67 | −1.56 | 0.00 (*NM) | 2.44 | 2.02 | 2.68 |
| $MoS_2\_3N_S$ | −2.47 | 1.62 | −2.23 | 0.00 (NM) | 2.43 | 2.04 | 2.66 |
| $MoS_2\_1N_{Mo}$ | −8.07 | 1.18 | −0.84 | 0.34 (0.82) | 2.39 | 1.78 | 3.11 |
| $MoS_2\_1N_{Mo}\_1N_S$ | −11.49 | 0.94 | −1.72 | 0.00 (NM) | 2.35 | 1.92 | 2.74 |
| $MoS_2\_1V_S\_1N_S$ | −1.92 | 0.90 | −0.95 | 0.17 (0.61) | 2.38 | 2.01 | 2.70 |
| $MoS_2\_1V_{Mo}\_3N_S$ | −8.05 | 0.91 | −2.21 | 0.20 (2.20) | 2.43 | 1.93 | 2.63 |

[a] $E_g$ is the calculated direct energy band gap
[b] $Q_N$ stands for total charge obtained by the N atoms. Negative charge means charge was transferred from $MoS_2$ surface atoms to the N atom, and vice versa.
[c] $M_N$, is the net magnetic moment of the N dopant atoms. The values in brackets are the net magnet moment of the entire structure.
[d] $d_{Mo-S}$, is the average distance between Mo and S atoms close to the defect sites.
[e] $d_{N-Mo}$, is the average distance between the N atom and its neighboring Mo atoms.
[f] $h_{N-S}$, is the height of the N atom with respect to the S plane (that is, S atom of the S-layer opposite to the layer doped with N atom).
[*] NM, means nonmagnetic state, which shows that the investigated model exhibits a nonmagnetic state (i.e. total magnetic moment, $\mu = 0\ \mu_B$).

to fewer N atoms. The reason is that the replacement of Mo and/or S atoms in the $MoS_2$ sheet by N atoms ($MoS_2\_1N_{Mo}\_1N_S$ and $MoS_2\_1N_{Mo}$), further creates a local reconstruction on the S layer in adjacent site (Fig. 1) in an energetically favorable manner during optimization (see S3.1 in the Supporting Information).

From Table 1, it can be observed that the average N—Mo bond length shows a small increase with the number of N dopants for both vacant and non-vacant systems. Specifically, the $MoS_2\_1V_s\_1N_S$ system exhibited a N—Mo bond length of 2.01 Å, which is similar to that of non-defective configurations despite containing an S vacancy. This can be related to the characteristic stretching of the Mo—Mo distance within the vicinity of the S vacant site, which offers a cushioning effect on the N—Mo bond by the vacancy site upon optimization. On the contrary, $h_{N\text{-}S}$ (the height of the nitrogen atom with respect to the S atoms) decreases with increasing numbers of N dopants for the systems. $MoS_2\_1N_{Mo}$ displayed the largest $h_{N\text{-}S}$ value of *approx.* 3.11 Å, which is close to the interlayer S-S distance of pristine $MoS_2$ (3.11 Å). This can be associated with the shortest $d_{N\text{-}Mo}$ for $MoS_2\_1N_{Mo}$ when compared to the other structures. Overall, our results showed that the vacancy defects (single or double) created in $MoS_2$ do not induce molecular structure reconstruction as witnessed in the case of carbon vacancy in graphene [40]. The comprehensive details of the binding energy and bond lengths is given in Supporting Information (Section S3.1).

The electron transfer between the dopant and the surface was also investigated by examining the charge densities using Bader charge analysis [36]. As can be seen from Table 1, the values of $Q_N$ are negative for all the considered surfaces, which indicates that the transfer of electrons occurred from the surficial atoms to the N atom. As discussed in the Supporting Information (S3.2), this is in line with the electronegative nature of the N atom [41]. The Pauling electronegativity of both Mo and S atoms of the surface are 2.16 and 2.58, respectively, which are smaller than 3.04 for the N atom. Hence, charge transfers from the Mo and S atoms to N dopant, which becomes more negatively charged. The charge transfer from the surface to the N dopant increased with the number of N atoms present in the structure and, there is charge transfer from the 1 S-vacancy sites to the N dopant. In addition, the results from Table 1 show that $MoS_2\_1N_S$, $MoS_2\_1V_S\_1N_S$, $MoS_2\_1N_{Mo}$ and $MoS_2\_1V_{Mo}\_3N_S$ exhibit a magnetic moment. This is because of the fewer number of N atoms in $MoS_2\_1N_S$ and the vacancy in $MoS_2\_1V_S\_1N_S$, $MoS_2\_1N_{Mo}$ and $MoS_2\_1V_{Mo}\_3N_S$. In contrast, $MoS_2\_2N_S$, $MoS_2\_3N_S$ and $MoS_2\_1N_{Mo}\_1N_S$ (with higher number of N atoms) exhibit a nonmagnetic moment despite having double the amount of charge transfer that could enable significant disturbance and spin polarization. It is also observed that the excess charge transfer around the N dopants is evenly distributed among the N atoms. This even distribution reduces the effect of spin polarization on the surface, and thus, do not induce a magnetic moment. The distribution of the magnetic moment can be clearly seen from Fig. 2, which is the isosurfaces of the spin charge density difference for the defective $MoS_2$ monolayer, $\Delta\rho_s$, and was obtained using Equation (S4) as explained in the Supporting Information (S1.3). More details on charge transfer and magnetic properties are discussed in the Supporting Information (Section S3.2).

Finally, to provide more insight into the electronic properties of these sites, the total (TDOS) and partial (PDOS) density of state were calculated. Fig. 3 presents the characteristic TDOS and PDOS of the N-doped vacancy free and N-doped vacancy containing $MoS_2$ monolayers. N is expected to act as a source of p-type doping for the monolayer $MoS_2$ when it substitutes for S, due to that N have one p valence electron less than S. This leads to the generation of a hole in the valence band as shown in the DOS plots (Fig. 3). The calculated direct energy band gap ($E_g$) for each structure is given in Table 1. From Table 1, the band gaps become narrower as the number of N dopants increases for the N-doped vacancy-free systems. The narrow state of the band gap compared with the pristine structure (1.79 eV) indicates a shift in the Fermi level is mainly due to the impurity state introduced by N atoms. The impurity states mainly come from the hybridization between the 2p orbitals of N and the 4d orbitals of its neighboring Mo. The electron transfer due to the presence of nitrogen as a p-type dopant and the band bending induced by the formation of Mo—N covalent bond at the top-most layer, as well as the preferential sulfur removal, contribute to a band shift, which is commonly found in N doped $MoS_2$ [11,42]. Furthermore, it is observed that much narrower band gaps are obtained in N doped single S or Mo vacancy defect complexes. This can be attributed to the combined effects of the impurity state introduced by N atom as a p-type

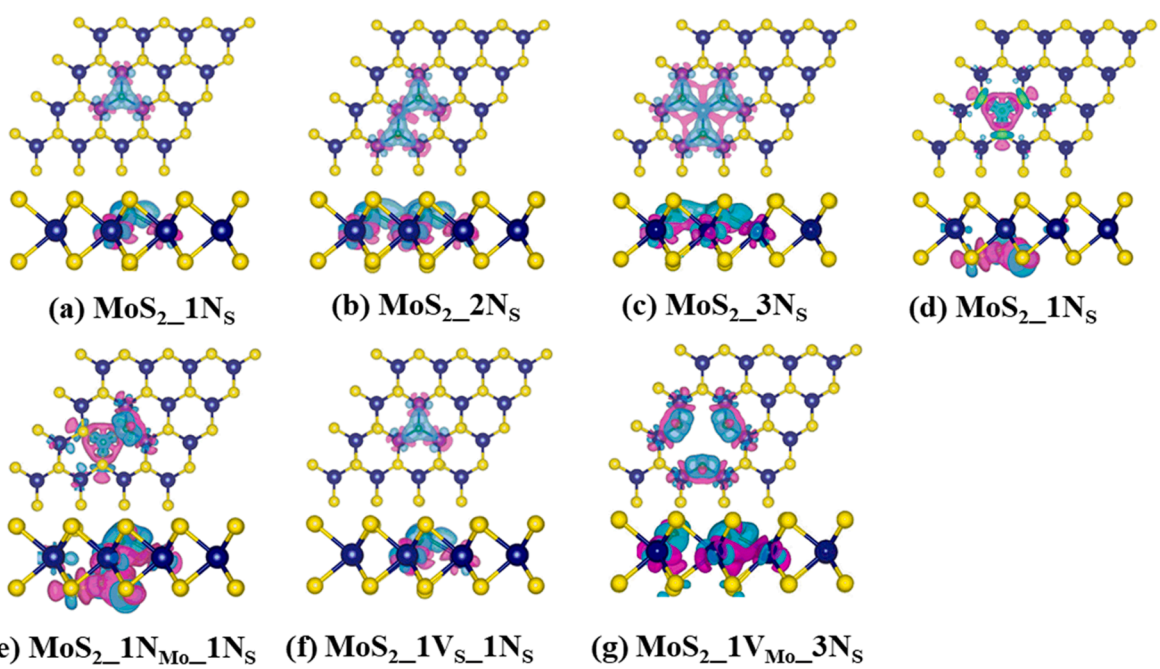


**Fig. 2.** Top and side views of isosurfaces of spin density difference for the defect surfaces with isosurface taken as ±0.005 e/Bohr$^3$. The light blue and pink colors represent areas with increase and decrease of electron density, respectively. The color codes for Mo, S and N atoms are the same as in Fig. 1. (For interpretation of the references to colour in this figure legend, the reader is referred to the web version of this article.)

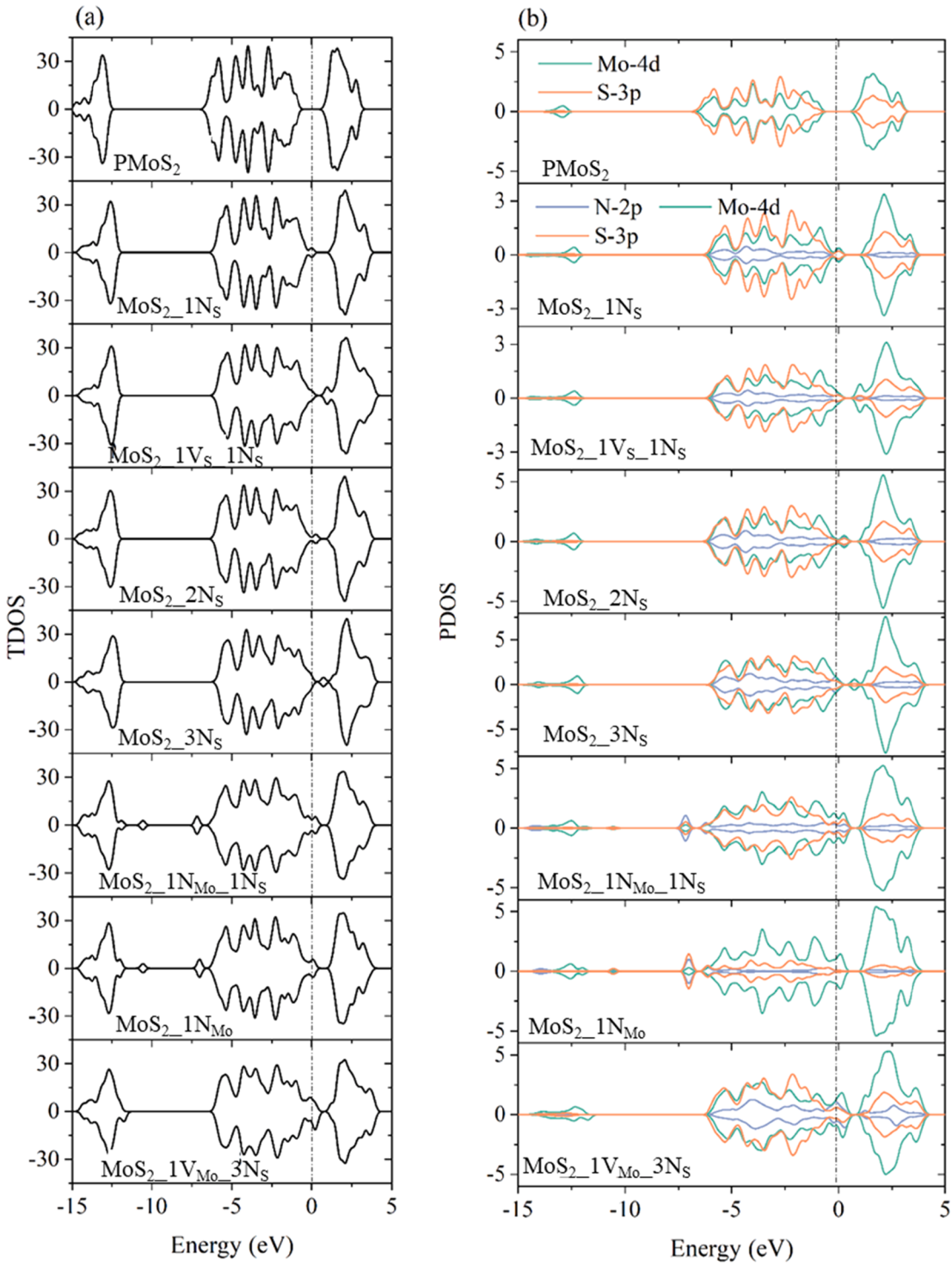


**Fig. 3.** (a) The TDOS of the defect-free and N doped monolayer $MoS_2$. (b) The PDOS projected on the 3p orbitals of N dopants and the 3p and 4d orbitals of their neighboring S and Mo atoms, respectively. The positive and negative values of DOS illustrate the spin-up and spin-down states, respectively. Green, orange and blue lines represent 4d, 2p and 3p orbitals, respectively. The Fermi level is represented by the vertical dashed line. (For interpretation of the references to colour in this figure legend, the reader is referred to the web version of this article.)

dopant and the defect states as a result of unsaturated S or Mo atoms near the single S or Mo vacancy, respectively [29]. A detailed explanation of the defect states in non-doped single S or Mo vacancy defect is provided in Section S2 of the Supporting Information.

### 3.2. $CO_2$ adsorption on the considered $MoS_2$ surfaces

To investigate the adsorption of $CO_2$ on the pristine or defect (vacancy or N-substitutional doping) monolayer $MoS_2$, the adsorption energy ($E_{AE}$) is calculated using Equation (S5) as described in the Supporting Information (S1.3). The molecular height is defined as the distance between the carbon atom of the $CO_2$ molecule and a reference

atom of the $MoS_2$ surface in the basal plane in the z-direction (i.e. N atom for N doped $MoS_2$ surface and average z plane of S atoms, for non-doped $MoS_2$ surface). It should be pointed out that top (Mo or S), hollow or bridge sites of the $MoS_2$ monolayer were not emphasized in our calculations. The reason for this is that a theoretical study has shown that $MoS_2$ is a poor adsorbent for $CO_2$ irrespective of these sites, but defective $MoS_2$ is a good adsorbent, hence, our focus is to further enhance the adsorption by N doping [19]. In this regard, the $CO_2$ molecule was initially placed at a height of 2.5 Å from S or Mo at the vacancy site and doped N atom(s) for vacancy defect and N-doped monolayer $MoS_2$, respectively. Different orientations of the $CO_2$ molecule and lateral positions with respect to XYZ axes of the $MoS_2$ supercell were also considered in order to obtain the most stable $CO_2$ adsorption configurations.

Based on the test calculations (Table S2), only the most stable relaxed adsorption geometric structures and results are presented and discussed here, while the others can be found in the Supporting Information (Section S5). Fig. 4 presents the schematic structure of the most stable $CO_2$ adsorption configurations for the pristine or defect (vacancy or N-substitutional doping) monolayer $MoS_2$. Except for the $MoS_2\_1V_S$, all other models exhibited a stable $CO_2$ adsorption when the $CO_2$ molecule is oriented in parallel with the surface of the model. It is worth mentioning that $MoS_2\_1N_{Mo}$ is not a stable adsorption configuration for $CO_2$ molecule due to a high positive adsorption energy in all the considered configurations (Table S3), therefore is not be discussed further.

Further elaboration of the adsorption properties at 2.5 Å initial molecular height is given in Table 2. Table 2 presents the equilibrium molecular distance between the adsorbate and the substrate yielded by optimization ($h_{mol\text{-}surf}$), along with the corresponding adsorption energy ($E_{AE}$) and characteristic parameters for the considered models such as the amount of charge transfer (from Bader charge analysis) between $MoS_2$ and $CO_2$ molecule ($Q_{CO2}$), and $MoS_2$ and nitrogen atom of the dopant ($Q_N$), characteristic surficial bond lengths ($d_{Mo\text{-}S}$, $d_{N\text{-}Mo}$ and $h_{N\text{-}S}$,) average bond lengths (l) and bond angles (θ) of $CO_2$ after adsorption, and change in $CO_2$ bond angles (Δθ). Δθ is the difference between the bond angle experimental value (180°) [43] and the value obtained from the structural optimization. For example, a stable $CO_2$ adsorption on the $MoS_2\_1N_S$ surface displayed an equilibrium height of 3.085 Å with an adsorption energy of −0.197 eV. All equilibrium heights obtained from the models are lower than that obtained in $PMoS_2$ (3.456 Å) with an adsorption energy of 0.139 eV. As shown in Table 2, $MoS_2\_1V_{Mo}\_3N_S$ (3.313 Å) gives highest adsorption energy of 1.818 eV, which is 13 times higher than that of $PMoS_2$. Also, $CO_2$ is considered to be physisorbed on all the surfaces based on the large separation heights, except for $MoS_2\_1V_S$ surface, where $CO_2$ molecule was found to undergo a dissociative adsorption. The detailed discussion on the dissociation is given in the subsequent section.

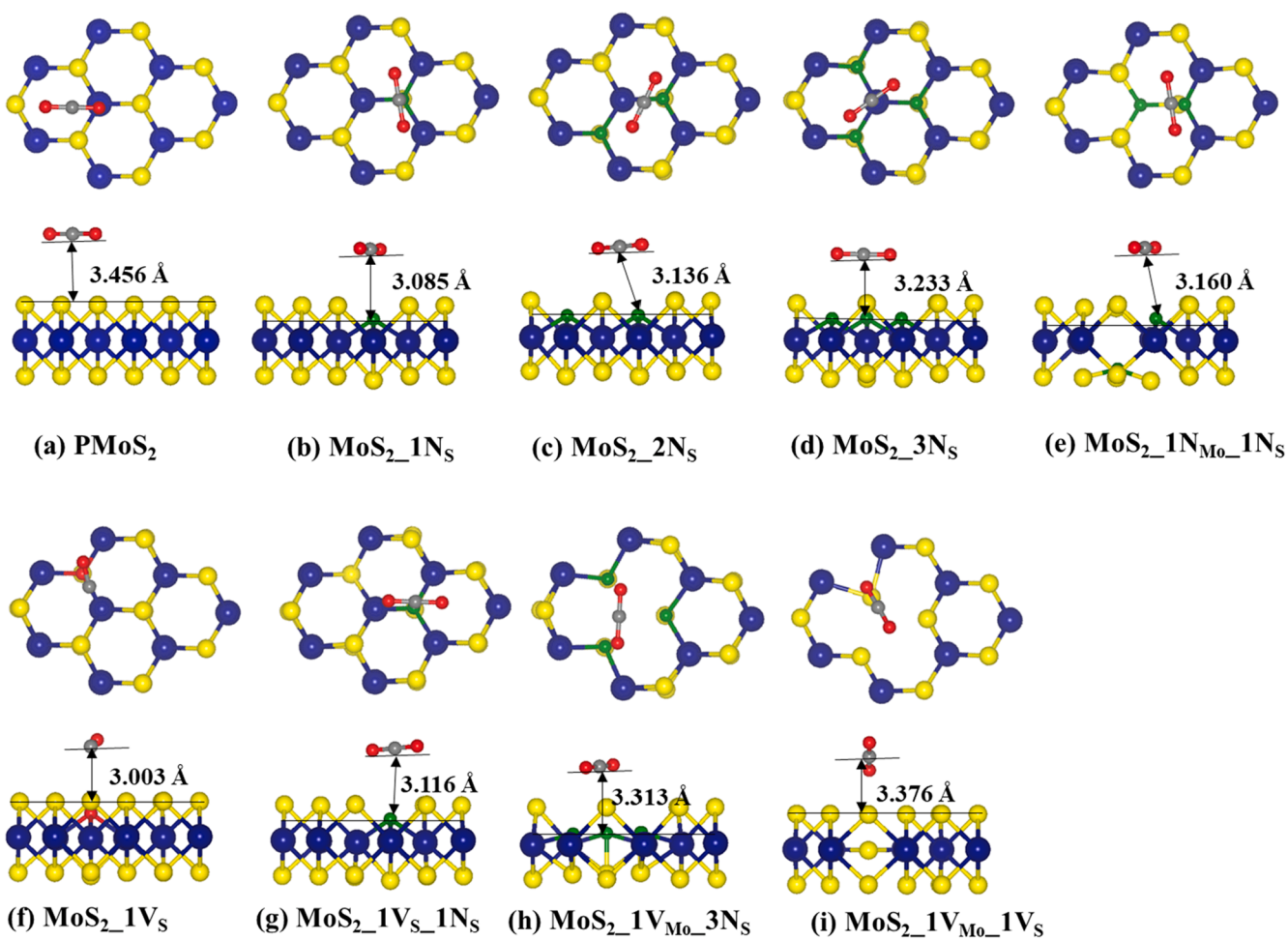


**Fig. 4.** The schematic structure of the most stable adsorption configurations for $CO_2$ molecule adsorbed on the pristine and defect (vacancy or N-substitutional doping) monolayer $MoS_2$ from top (upper panel) and side (lower panel) views. The full descriptions of a–i have been given in Fig. 1. The color codes for Mo, S and N atoms are the same as in Fig. 1, while, O and C atoms are shown in red and grey, respectively. The lines define the equilibrium molecular height between the central carbon atom of the $CO_2$ molecule and a reference atom of the $MoS_2$ surface in the basal plane in the z-direction yielded by optimization (i.e. N atom for N doped $MoS_2$ surface and average z plane of S atoms, for non-doped $MoS_2$ surface given in Å.

**Table 2**
Summary of calculated results for adsorption of $CO_2$ on most stable configurations of different surfaces at 2.5 Å initial molecular height.

| Model | $E_{AE}$, eV | $Q_{CO2}$ [a], e | $Q_N$ [b], e | [c] $M_N$, $\mu_B$ | $h_{mol\text{-}surf}$ [d], Å | $d_{Mo\text{-}S}$ [e], Å | $d_{N\text{-}Mo}$ [f], Å | $h_{N\text{-}S}$ [g], Å | l, Å | θ, ° | Δθ, ° |
|---|---|---|---|---|---|---|---|---|---|---|---|
| $PMoS_2$ | −0.139 | −0.020 | – | – | 3.456 | 2.412 | – | – | 1.177 | 179.698 | 0.302 |
| $MoS_2\_1N_S$ | −0.197 | −0.017 | −0.958 | 0.213 (0.840) | 3.085 | 2.443 | 2.019 | 2.694 | 1.177 | 178.713 | 1.287 |
| $MoS_2\_2N_S$ | −0.200 | −0.017 | −1.894 | 0.000 (* NM) | 3.136 | 2.439 | 2.012 | 2.681 | 1.177 | 178.712 | 1.288 |
| $MoS_2\_3N_S$ | −0.211 | −0.015 | −2.814 | 0.000 (NM) | 3.233 | 2.365 | 2.016 | 2.655 | 1.176 | 178.710 | 1.290 |
| $MoS_2\_1N_{Mo}\_1N_S$ | −0.186 | −0.019 | −1.702 | 0.000 (NM) | 3.160 | 2.351 | 1.926 | 2.754 | 1.176 | 178.720 | 1.280 |
| $MoS_2\_1V^*_S$ | −0.908 | [h] −1.015 (0.109) | – | – | [i] 3.003 | 2.421 | – | – | 1.144 | – | – |
| $MoS_2\_V_S\_1N_S$ | −0.196 | −0.019 | −0.962 | 0.089 (0.544) | 3.116 | 2.384 | 2.016 | 2.699 | 1.176 | 178.975 | 1.025 |
| $MoS_2\_1V_{Mo}\_3N_S$ | −1.818 | −0.012 | −2.557 | 0.027 (0.256) | 3.313 | 2.365 | 2.046 | [‡] 1.776 | 1.177 | 178.581 | 1.419 |
| $MoS_2\_1V_{Mo}\_1V_S$ | −0.252 | −0.027 | – | – | 3.376 | 2.334 | – | – | 1.179 | 179.369 | 0.631 |

[a] $Q_{CO2}$.
[b] $Q_N$, are total charge obtained by the $CO_2$ molecule and N atom of the dopant respectively. Negative charge means charge is transfered from $MoS_2$ surface atoms to the atoms of $CO_2$ molecule, and vice versa.
[c] $M_N$, is the net magnetic moment of the N dopant atoms. The values in brackets are the net magnet moment of the entire structure.
[d] $h_{mol\text{-}surf,}$ is the equilibrium molecular height, the equilibrium molecular height is the height between the central carbon atom of the adsorbed $CO_2$ molecule and a reference atom of the $MoS_2$ surface in the basal plane in the z-direction yielded by optimization (That is, N atom, for N doped $MoS_2$ surface and average z plane of top S-layer atom, for non-doped $MoS_2$ surface).
[e] $d_{Mo\text{-}S}$, is the average distance between Mo and S atoms close to the defect sites nearest to the adsorbed $CO_2$.
[f] $d_{N\text{-}Mo,}$ is the average distance between the N atom and its neighboring Mo atoms nearest to the adsorbed $CO_2$.
[g] $h_{N\text{-}S,}$ is the height of the N atom with respect to the S plane (that is, S atom of the S-layer opposite to the layer doped with N atom).
[*] $MoS_2\_1V_S$ model, however might not be a stable system for sustainable $CO_2$ adsorption because of the strong tendency of one O atom of $CO_2$ to embed in the $MoS_2$ surface, thus creating Mo-O-Mo layer at the S vacancy site when the $CO_2$ molecule is oriented vertically leading to the formation of CO gas, therefore, the adsorption energy presented there is rather $CO_2$ dissociation energy.
[h] -1.015 (0.109) e, is the charge gained (lost) by the formed CO gas (O atom that bonded with the surface).
[i] 3.003 Å, is the distance between C atom of the formed CO gas and O atom that bonded with the surface.
[‡] 1.776 Å, is the average N-S triple bond length, that is, when $CO_2$ adsorbed on $MoS_2\_1V_{Mo}\_3N_S$ surface, triple bonds were formed between opposite dangling N and S atoms in the Mo vacancy.*NM, means nonmagnetic state, which shows that the investigated model exhibits a nonmagnetic state (i.e. total magnetic moment, $\mu = 0\ \mu_B$).

### 3.3. $CO_2$ adsorption on defective $MoS_2$ monolayer

For $MoS_2\_1V_S$, an improved adsorption efficiency of $CO_2$ is obtained with an adsorption energy of −0.908 eV. This energy is much stronger than those obtained for $CO_2$ interaction with some MOFs or carbon-based nanomaterials [44,45]. As discussed earlier, only the $MoS_2\_1V_S$ model exhibited the dissociation of $CO_2$ to yield lattice-embedded oxygen and CO molecule that desorb from the surface at the considered molecular height (Fig. 4f). The dissociative chemisorption of $CO_2$ on the single S vacancy defect can be associated with the perpendicular orientation of $CO_2$ molecule and the increased covalent attractions. The covalent attraction was observed to be higher around the vacancy defect sites due to the three dangling Mo atoms. The O atom of the $CO_2$ molecule possesses excess negative charge due to its higher electronegativity when compared to the central C atom. As a result, the O atom is strongly attracted to the more positively charged vacant site, due to the enhanced charge transfer from the excess positively charged dangling Mo atoms ($Q_{Mo} = 0.07$ e) to the single S-vacancy defect sites (Table S2).

This explains why the $CO_2$ molecule tends to distance itself from the vicinity of single S vacancy defect of $MoS_2$ monolayer when linear $CO_2$ is placed horizontally along the z-axis, since the positively charged central C atom of $CO_2$ is not electrostatically attracted to the positively charged dangling Mo atoms of single S vacancy defect. As a result, the large electropositive central C atom may make it difficult for $CO_2$ to grab electrons from the $MoS_2\_1V_S$ defect site and thus prevent the strong interaction between them. As shown in Table S3, the repulsive interaction between $CO_2$ and $MoS_2\_1V_S$ when linear $CO_2$ molecule is horizontally oriented along the z-axis is reflected in the positive adsorption energy. This is one reason why pristine $MoS_2$ surface does not strongly interact with $CO_2$ molecule as the layer of negatively charged S atoms shields the inner positively charged Mo atoms. Subsequently, a lesser interaction is observed on the pristine surface when $CO_2$ is perpendicularly oriented to the surface. The calculated energy of −0.908 eV is far larger than the value reported in Ref. [21] for $CO_2$ adsorption on the single SV defect site. This reported study suggested that $CO_2$ only physisorbed on $MoS_2\_1V_S$. Part of the discrepancy can be attributed to the perpendicularly orientated $CO_2$ molecule and the effect of lateral interaction between the O of $CO_2$ pointing towards the S vacant site and the surface.

Furthermore, as shown in Fig. 4f, the lattice-embedded oxygen and three dangling Mo atoms are linked by three newly formed O—Mo covalent bonds, whose average length is 2.081 Å, shorter than the Mo-S bond length. The formation of these bonds leads to the elongation of the surrounding Mo-S bonds from 2.412 to 2.421 Å as shown in Table 2. Bader Charge analysis shows 0.109 e charge transferred from the lattice-embedded oxygen to the detached CO, which obtained 1.015 e total electron charge. The distance between C atom of the detached CO molecule and the lattice-embedded O atom is 3.003 Å. This value is smaller than 3.500 Å reported in Ref. [26] for CO physisorption on perfect $MoS_2$ surface, which indicates a strong physisorption state. The C—O bond length is calculated to be 1.114 Å, which is in excellent agreement with the experimental value of 1.13 Å [43].

Pertaining to $MoS_2\_1V_{Mo}\_1Vs$, the adsorption of $CO_2$ resulted in a moderate adsorption energy of −0.252 eV, which corresponds to a physisorption process. $CO_2$ physisorption is therefore energetically favored in $MoS_2\_1V_{Mo}\_1Vs$ by −0.113 eV over the $PMoS_2$ and notably lesser by −0.656 eV when compared to the dissociative adsorption on $MoS_2\_1V_S$. The large difference in the adsorption energies between $MoS_2\_1V_S$ and $MoS_2\_1V_{Mo}\_1Vs$ can be attributed to the missing Mo atom in $MoS_2\_1V_{Mo}\_1Vs$ surface, which reduces the electrostatic and covalent components of the interaction between the O atom of $CO_2$ and the vacant site. The adsorption distance of $MoS_2\_1V_{Mo}\_1Vs$ is 3.376 Å, which is also shorter than that obtained for $PMoS_2$, and the $CO_2$ molecule adopts a tilted orientation, with O atom pointing to the MoS defect as shown in Fig. 4i. The bond length of the physisorbed $CO_2$ slightly increased while the bond angle decreased by ~0.6° with respect to the linear $CO_2$ in gas phase (Table 2). From the Bader charge analysis, 0.027 e charge is transferred from $MoS_2\_1V_{Mo}\_1Vs$ surface to $CO_2$ molecule, which is comparable to that obtained with the prefect surface. Thus, this proves that $CO_2$ molecule gives a moderate interaction with $MoS_2\_1V_{Mo}\_1Vs$ defect. The calculated adsorption energy of −0.252 eV is close to the value of −20.5 kJ/mol (-0.213 eV) reported by Ref. [19].

To analyze the electronic properties of the defect structures upon

$CO_2$ adsorption, the density of state (DOS) and charge density difference were calculated. The charge density difference, $\Delta\rho_{df}$, is defined in the Supporting Information (S1.3) using Equation (S6). Fig. 5 presents the TDOS and PDOS of the adsorption system. The PDOS were projected on the relevant orbitals: p and d orbitals of the respective S and Mo atoms near the MoS and S vacancy sites, p orbital of N dopants, and the s and p orbitals of the CO and $CO_2$ molecules, and lattice embedded O atom. As can be seen in Fig. 5b, when $CO_2$ physisorbed on the MoS vacancy site ($MoS_2\_1V_{Mo}\_1V_S$), there is an orbital coupling between the p orbital of $CO_2$ and the d orbital of the Mo atom, which is in agreement with a previous study [19]. There are no significant changes in the DOS spectra of either valence or conduction band of $MoS_2\_1V_{Mo}\_1V_S$ upon $CO_2$ adsorption just like in the perfect surface (Fig. S2b). The narrower band gap near the Fermi level when compared to the pristine surface, is due to the defect states introduced as a result of vacancy formation (see Supporting Information). Contrarily, after $CO_2$ dissociated on $MoS_2\_1V_{Mo}\_1V_S$, the lattice embedded O atom acts as a coverage on the S vacancy site, thus there is a modification of the band gap near the Fermi level (see Fig. 5a). The defect states introduced as a result of unsaturated Mo atoms near the 1 S-vacancy, is now eliminated by the lattice embedded O atom, forming 3 saturated Mo—O bonds. Hence, the band gap near the Fermi level of this stable structure is normalized and compares with that of the perfect surface. This result agrees with reported studies that atmospheric oxygen heals vacancies and other defects resulting from sulfur vacancy in $MoS_2$ [46,47].

The isosurfaces of spin density difference for the $CO_2$ molecule adsorption on the defect surfaces ($MoS_2\_1V_S$ and $MoS_2\_1V_{Mo}\_1V_S$) are presented in Fig. 6. There is a charge difference re-distribution in the middle region between $CO_2$ molecule and $MoS_2\_1V_{Mo}\_1V_S$ substrate (Fig. 6b), with much noticeable polarization of the $MoS_2\_1V_{Mo}\_1V_S$ sheet upon $CO_2$ adsorption. This indicates a stronger covalent character, when compared to the perfect surface (Fig. S2a). This explains why the $MoS_2\_1V_{Mo}\_1V_S$ gives a higher adsorption energy than the $PMoS_2$. Meanwhile, there is more charge transfer and stronger interaction between the $MoS_2\_1V_S$ surface with the lattice-embedded O atom and CO molecule (Fig. 6a), which can be compared to that of Lewis acid interaction. The electrophilic C atom of CO makes the molecule Lewis acidic and interacts with lattice embedded O atom through electron acceptor-donor type interaction. A total electron charge of about 1.015 e is transferred from the surface to the CO molecule, with the embedded O atom contributing a considerable 0.109 e. The interaction of CO with the $MoS_2\_1V_S$ is favored by −0.968 e when compared to the total amount charge received by $CO_2$ molecule from both $PMoS_2$ and $MoS_2\_1V_{Mo}\_1V_S$ vacancy surfaces. The high amount of charge transfer to the CO molecule and the stability of electronic structure of 1 S-vacancy $MoS_2$ due to the presence of O atom provides evidence of n-type doping, and the effect of O atom on stabilizing the electronic properties $MoS_2$. Hence, this large electron transfer significantly changes the electronic transport properties of $MoS_2\_1V_S$.

### 3.4. $CO_2$ adsorption on N-doped defected $MoS_2$ monolayer

From the results presented in Table 2, it is evident that the $MoS_2\_1V_{Mo}\_3N_S$ site possesses the highest activity for $CO_2$ adsorption ($E_{AE} = -1.818$ eV) amongst all of the considered N-doped models, which is significantly higher than the defective $MoS_2$ monolayers ($MoS_2\_1V_S$ and $MoS_2\_1V_{Mo}\_1V_S$). Therefore, to understand the effect of nitrogen doping on vacancy $MoS_2$, the adsorption characteristic of $MoS_2\_1V_{Mo}\_3N_S$ is investigated. Also, the adsorption properties of $CO_2$ molecule on $MoS_2\_1V_{Mo}\_3N_S$ sites are calculated and compared with that of the perfect $MoS_2$ and non-doped vacancy surfaces. As shown in Fig. 4, $CO_2$ physisorbed on $MoS_2\_1V_{Mo}\_3N_S$ has an equilibrium molecular height of 3.313 Å with its molecular axis parallel to the $MoS_2\_1V_{Mo}\_3N_S$ basal plane. This parallel adsorption configuration is similar to that of $CO_2$ adsorption on the pristine $MoS_2$ surface, except that the $CO_2$ physisorbed on the perfect surface displayed an equilibrium molecular height of 3.456 Å. The physisorption of $CO_2$ molecule on the N doped vacancy site stretches out the surficial N atoms resulting in an increase in $d_{N\text{-}Mo}$ from 1.93 Å (Table 1) to 2.046 Å (Tables 2).

The interaction between $CO_2$ and $MoS_2\_1V_{Mo}\_3N_S$ surface yields stronger $CO_2$-surface interactions compared to pristine $MoS_2$ ($PMoS_2$) or the other defect (vacancy or N-substitutional doping) sites. Specifically, the $CO_2$ adsorption physisorption energy is approximately 13 times as strong as that on a $PMoS_2$. The superior adsorption performance is also illustrated by the difference in the equilibrium molecular height between $MoS_2\_1V_{Mo}\_3N_S$ and $PMoS_2$. The difference can be explained by their bonding nature with $CO_2$. The positively charged central carbon atom of $CO_2$ molecule is attracted electrostatically to the negatively charged tertiary nitrogen atoms surrounding the Mo vacancy. The absence of an Mo atom lessens the repulsive component of the interaction. As shown in Table S2, the adsorption energetic configuration for $CO_2$ molecule on $MoS_2\_1V_{Mo}\_3N_S$ is obtained when the linear $CO_2$ molecular axis is placed parallel to the surface. Less or repulsive interaction is observed when linear $CO_2$ is perpendicularly oriented to the surface, with the O atom pointing to the $MoS_2$ basal plane. The result indicates that for pristine $MoS_2$ surface, $CO_2$ physisorption mainly occur on the basal plane through van der Waals interaction, whereas the N atoms surrounding the Mo vacancy site in $MoS_2\_1V_{Mo}\_3N_S$ promotes the physical interaction between $CO_2$ molecules through non-covalent interaction and enhanced electrostatic interaction on the N doped Mo

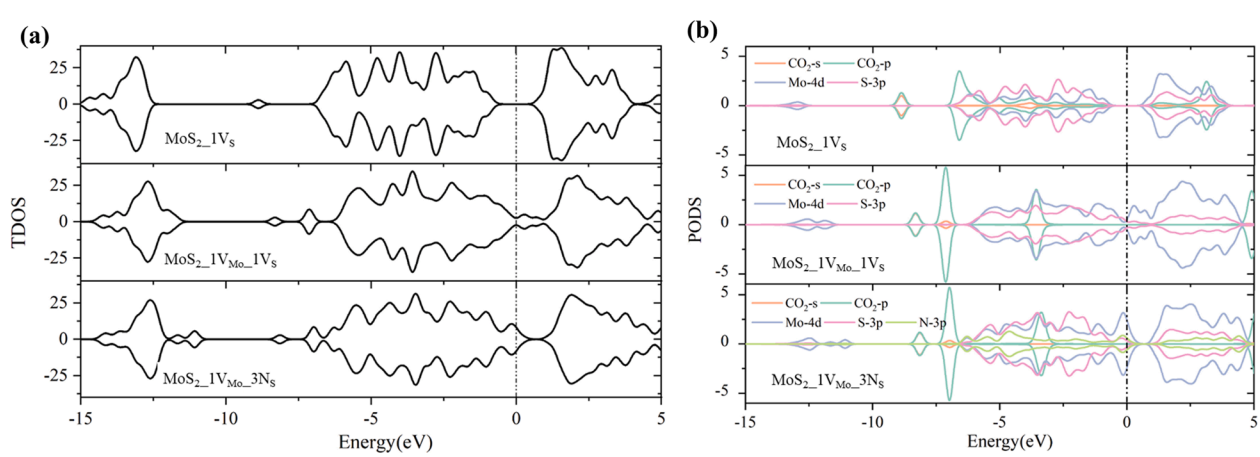


**Fig. 5.** (a) The TDOS and (b) The PDOS projected on the p and d orbitals of respective S and Mo atoms near to the MoS and S vacancy sites, p orbital of N dopants and the s and p orbitals of the physorbed CO and $CO_2$ molecules, and lattice embedded O atom. $MoS_2\_1V_S$, $MoS_2\_1V_{Mo}\_1V_S$ and $MoS_2\_1V_{Mo}\_3N_S$ represent 1 S-vacancy, 1Mo- and 1S-vacancy, and tertiary nitrogen doped 1 Mo-vacancy $MoS_2$ monolayers, respectively. The vertical dashed line corresponds to the Fermi level.

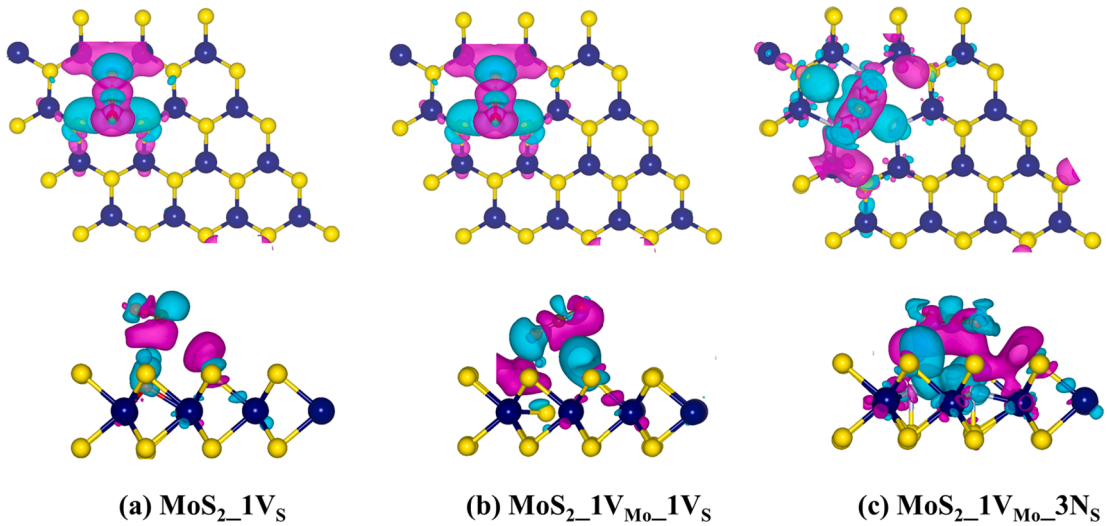


**Fig. 6.** Top and side views of isosurfaces of spin density difference of (a) 1 S-vacancy, (b) 1 Mo and 1 S vacancy and (c) tertiary nitrogen doped 1 Mo-vacancy, with isosurface taken as ±0.00015 e/Bohr$^3$. The light blue and pink colors represent increase and decrease of electron density, respectively. (For interpretation of the references to colour in this figure legend, the reader is referred to the web version of this article.)

vacancy sites. This result demonstrates that N doping could boost the effective surface for $CO_2$ adsorption by facilitating both van der Waals and electrostatic interactions. This phenomenon is quite similar to $CO_2$ physisorption on N doped carbon surface [48].

Furthermore, the geometric structures of $CO_2$ molecule adsorbed on $MoS_2$_1$V_{Mo}$_3$N_S$ were calculated to understand the surface-molecule interactions. The bond length and bond angle of the physisorbed $CO_2$ molecule were calculated and compared related to the values in gas phase. As shown in Table 2, the bond angle of the physisorbed $CO_2$ molecule changed compared to the gas phase $CO_2$. The calculated bond angle of physisorbed $CO_2$ is 178.68°, which decreased by 1.42° with respect to the gas phase $CO_2$ molecule [43]. The decrease in $CO_2$ bond angle makes the optimized state highly exothermic with a difference in adsorption energy of about −1.7 eV with respect to the pristine surface, where the bond angles remain almost unchanged after adsorption. Table 2 also shows that, the bond length of physisorbed $CO_2$ molecule are unchanged compared to the gas phase $CO_2$ molecule. Therefore, the geometric structure of $CO_2$ molecule is not affected when it is adsorbed on N doped 1 Mo-vacancy site, indicating only physical interaction.

Similar to the perfect and $MoS_2$_1$V_{Mo}$_1$V_S$ surfaces, the DOS analysis shows that there are no significant changes in the DOS spectra of either valence or conduction band of $MoS_2$_1$V_{Mo}$_3$N_S$ upon $CO_2$ adsorption. However, the band gap near the Fermi level was observed to be narrower than that for the pristine surface since the introduction of the N atom and 1 Mo-vacancy induces impurity and defect state, respectively, as explained in Section 3.1. The only observed effect of the adsorption is the orbital coupling between the p orbital of the $CO_2$ molecule and the d orbital of the Mo atom, as shown in Fig. 5b.

Bader charge analysis reveals that the interaction between the $CO_2$ molecule and $MoS_2$_1$V_{Mo}$_3$N_S$ surface also resulted in charge transfer and redistribution. As shown in Table 2, while 0.020 e is transferred to $CO_2$ in the pristine surface, only 0.012 e is transferred to $CO_2$ when 1 Mo-vacancy is doped with N atoms. The difference in the charge transfer supports the Lewis-acid interaction analogy between $CO_2$ and $MoS_2$_1$V_{Mo}$_3$N_S$ surface, but less noticeable when compared to the pristine and non-doped vacancy surfaces. Moreover, the reactive surface N atoms gain more electrons after $CO_2$ adsorption compared to the electrons gained by the N dopants before adsorption. Specifically, the total electron gained by the N dopant before and after $CO_2$ adsorption is 2.21 e (Table 1) and 2.557 e, respectively. Thus, the N dopants become more negatively charged after adsorption with an additional charge of 0.347 e. Also, as the surface N atoms become negatively charged, less charge is transferred to $CO_2$ molecule and higher adsorption energy is obtained, different from the behavior observed in pristine ($PMoS_2$) and non-doped vacancy ($MoS_2$_1$V_S$ and $MoS_2$_1$V_{Mo}$_1$V_S$) surfaces. This is attributed to the electron transfer from the oxygen atom of $CO_2$ molecules and indicates that $CO_2$ molecule binds strongly onto the N doped vacancy site by transferring some of the electrons of the O atom. These results further demonstrate that nitrogen doping of $MoS_2$ belongs to the p-type doping, which agrees with reference [42].

This conclusion drawn based on Bader charge analysis can be confirmed by the charge density difference, $\Delta\rho_{df}$. As shown in Fig. 6c, charge difference redistributes in the middle region between $CO_2$ molecule and $MoS_2$_1$V_{Mo}$_3$N_S$ substrate, with much more noticeable polarization of the $MoS_2$_1$V_{Mo}$_3$N_S$ sheet upon molecules adsorption, indicating a stronger covalent character, when compared to the perfect surface and the $MoS_2$_1$V_{Mo}$_1$V_S$. The light blue and pink colors represent increase and decrease of charge electron density, respectively. When $CO_2$ is physisorbed onto the surface, the reactive surface N atoms receive electrons from the region between the $CO_2$ central carbon atom and itself to strength the interaction between $CO_2$ and the surface. The increase in the pink color (decrease of electron density) in the middle region between the $CO_2$ and $MoS_2$_1$V_{Mo}$_3$N_S$ surface compared to the cases of defect-free and non-doped defective surfaces, indicates less charge transfer to $CO_2$ upon the adsorption on $MoS_2$_1$V_{Mo}$_3$N_S$. Also, the increase in the light blue color (increase of electron density) on the surface N atoms compared to $MoS_2$_1$V_{Mo}$_3$N_S$ surface before adsorption (Fig. 2), shows the reactive surface N atoms gained more electron after $CO_2$ adsorption. As a result, a large region of electron depletion appears near the oxygen atoms and there is lower electron density surrounding $CO_2$ compared to that of $CO_2$ in perfect surface (Fig. S2). For the magnetic properties, upon $CO_2$ adsorption, the magnetic moment of the surface N atom is significantly reduced to 0.027 $\mu_B$, while the net magnetic moment locates on the adsorbed $CO_2$ molecule as shown in Fig. 6c. This significant impact on the magnetic moment of $MoS_2$_1$V_{Mo}$_3$N_S$ upon $CO_2$ adsorption proposes that $MoS_2$_1$V_{Mo}$_3$N_S$ as a suitable $CO_2$ sensing device. These results suggest that, $CO_2$ interacts strongly with the Mo vacancy site, when the surrounding S atoms are substituted with N atoms. In general, the adsorption efficacy of the $MoS_2$ surface can be promoted by any measure that can enhance the electrostatic interaction between the $CO_2$ molecule and the surface complex, other than vdW interactions. This can be revealed by the electron charge distribution and magnetic moment-induced polarization. The qualitative difference between adsorption mechanisms associated with $CO_2$ on the perfect

surface and non-doped vacancy defect sites, and nitrogen doped Mo vacancy defect sites stresses the importance of nitrogen doping on vacancies for $CO_2$ adsorption in the $MoS_2$ system.

### 3.5. Infrared (IR) spectroscopy of CO2 adsorption on MoS2_1V$_S$, MoS2_1V$_{Mo}$_1V$_S$ and MoS2_1V$_{Mo}$_3N$_S$ surfaces

Calculation of the infrared (IR) spectroscopy of molecules adsorbed on the surface in conjunction with the experimental measurements can provide valuable approach to probe the structure of the surface absorbates. The vibrational frequencies of the $CO_2$ molecule adsorbed on $MoS_2$_1V$_S$, $MoS_2$_1V$_{Mo}$_1V$_S$ and $MoS_2$_1V$_{Mo}$_3N$_S$ surfaces were calculated and compared to the gas phase. As shown in Table 3, the vibrational frequencies of the asymmetric ($\nu3$) and symmetric ($\nu1$) stretching modes for gas phase $CO_2$ was calculated to be 2361 $cm^{-1}$ and 1328 $cm^{-1}$, respectively. The bending frequencies ($\nu2$) for gas phase $CO_2$ is calculated to be 633 $cm^{-1}$. The calculated value is in good agreement with the experimental value [43,49]. The discrepancies between the DFT calculated vibrational frequencies and the true vibrational frequencies arise from the harmonic treatment of the DFT vibrations and the inexact nature of DFT in solving the Schrödinger equation, which are common in quantum chemistry calculations [50]. To correct the discrepancies, the DFT results are often multiplied by a scaling factor (in the range of 0.95–0.99 for typical GGA) to match the experimental measurements [50]. In this study, we used scaling factor of 0.989.

The computed asymmetric stretching modes ($\nu3$) for physisorbed $CO_2$ molecule on $MoS_2$_1V$_{Mo}$_1V$_S$ and $MoS_2$_1V$_{Mo}$_3N$_S$ surfaces are 2353 $cm^{-1}$ and 2355 $cm^{-1}$, respectively. These values downshifts by 8 $cm^{-1}$ and 6 $cm^{-1}$ to the value calculated in gas phase $CO_2$. The calculated symmetric stretching modes ($\nu1$) for physisorbed $CO_2$ on $MoS_2$_1V$_{Mo}$_3N$_S$ surface, 1317 $cm^{-1}$, downshifts by 11 $cm^{-1}$ with respect to the calculated symmetric stretching mode of gas phase $CO_2$. The calculated symmetric stretching mode for physisorbed $CO_2$ on $MoS_2$_1V$_{Mo}$_1V$_S$ is 1315 $cm^{-1}$, which downshifts by 13 $cm^{-1}$ with respect to the calculated symmetric stretching mode of $CO_2$ in the gas phase. The slight downshift in the vibrational frequencies of the physisorbed $CO_2$ molecule indicates that the C═O bonds are slightly weaken when $CO_2$ molecule interact with $MoS_2$_1V$_{Mo}$_1V$_S$ and $MoS_2$_1V$_{Mo}$_3N$_S$ sites.

Moreover, upon interaction with $MoS_2$_1V$_{Mo}$_3N$_S$ site, the $CO_2$ deformation mode ($\nu2$) of 633 $cm^{-1}$ remain unchanged with respect to the computed value in gas phase. Upon interacting with $MoS_2$_1V$_{Mo}$_1V$_S$ site, deformation mode ($\nu2$) of $CO_2$ is 623 $cm^{-1}$, which downshifts by 10 $cm^{-1}$ compared to the $\nu2$ mode in the gas phase. This downshift is responsible for the slight increase in C═O bond length as shown in Table 2. Together with the fact that the bond length and vibrational frequencies of $CO_2$ slightly changed, it can be concluded that C═O bonds are slightly weakened when $CO_2$ molecule is physisorbed on $MoS_2$_1V$_{Mo}$_1V$_S$ and $MoS_2$_1V$_{Mo}$_3N$_S$ sites. This confirms that there is no chemical bonding, and interactions are dominated by weak vdW forces.

We also calculated the vibrational mode of CO molecule formed upon $CO_2$ interaction with $MoS_2$_1V$_S$ site. The most intense frequency value, 2119 $cm^{-1}$, corresponds to C≡O stretching mode (Table 3), which is in excellent agreement with the experimental value [43,49]. This value is lower than the C═O bonds in the gas phase $CO_2$. In addition to the decrease in C—O bond length and the formation of triple bond, we can conclude that the dissociation of $CO_2$ on $MoS_2$_1V$_S$ site leads to the formation CO molecule. To the authors' knowledge, in terms of experimental and computational comparison, there are no direct vibrational frequencies of $CO_2$ molecule physisorbed on non-doped vacancy and tertiary N doped Mo vacancy $MoS_2$ sites. It is reasonable to compare the computed modes with $CO_2$ molecule in gas phase, in order to understand how these modes shifted upon interacting with the surfaces.

### 3.6. Selective adsorption of $CO_2$, $N_2$ and $H_2O$

An effective $CO_2$ adsorbent should selectively adsorb $CO_2$ molecule over other competitive gaseous molecules, such as $N_2$. Since our interest is on selectivity, only the binding energies of all the molecules on pristine and defect $MoS_2$ monolayer sites are compared and discussed here. This is important for testing the trapping and catalytic activity of the $MoS_2$ sites. All the calculated results for the most stable adsorption configurations of $N_2$ and $H_2O$ molecules on different surfaces are summarized in the Supporting Information (Table S10 and Table S11).

The highest adsorption energies between each substrate and the adsorbate ($CO_2$, $N_2$ and $H_2O$) are compared in Fig. 7a. It can be seen that the $N_2$ adsorption is weaker than $CO_2$ adsorption for all surfaces except $MoS_2$_1N$_{Mo}$_1N$_S$, in which $N_2$ is dissociated with a high dissociation energy rather than adsorbing on the surface. The weaker adsorption energy of $N_2$ is attributed to its smaller quadrupole moment and polarizability properties than those of $CO_2$. Also, $MoS_2$_1V$_S$ exhibits a weaker interaction with $N_2$ than pristine $MoS_2$ and the defective surfaces. The interaction between $N_2$ and $MoS_2$_1V$_S$ is repulsive as shown by the positive adsorption energy value, whereas $CO_2$ interacts exothermically with $MoS_2$_1V$_S$, leading dissociation of $CO_2$ molecule. This result implies that $MoS_2$_1V$_S$ is a good adsorbent for $CO_2$ activation and not effective for $N_2$ adsorption.

It is clear that the selective adsorption of $CO_2$ over $N_2$ is based on different binding affinities on the adsorbent surface. Therefore, the ratio and difference of the highest adsorption energies for $CO_2$ and $N_2$ can be indicators of selective adsorption (Fig. 7b). From Fig. 7b, $MoS_2$_1V$_S$ and $PMoS_2$ exhibit a relatively higher ratio of adsorption energy, while $MoS_2$_1N$_S$, $MoS_2$_2N$_S$, $MoS_2$_3N$_S$ and $MoS_2$_1V$_S$_1N$_S$ exhibit similar ratio of adsorption energy. The highest ratio of 5.1 is obtained for $MoS_2$_1V$_S$ surface, while the lowest ratio of 0.5 is obtained for $MoS_2$_1N$_{Mo}$_1N$_S$. Although the highest adsorption energies for $CO_2$ and $N_2$ molecules are obtained for $MoS_2$_1V$_{Mo}$_3N$_S$ structure as explained in the Supporting Information (S6), but smaller ratio of 1.0 compared to the values obtained for other structures. When the difference of adsorption energies for $CO_2$ and $N_2$ is compared, $MoS_2$_1V$_S$ site appears to be more suitable adsorbent for selective adsorption and separation of $CO_2$ over $N_2$.

The adsorption of an $H_2O$ molecule on the same surfaces are also compared to $CO_2$ adsorption to predict the stability of the defect and defect free $MoS_2$ monolayers towards $H_2O$ contaminant. Fig. 7c presents the ratio and difference of the highest adsorption energies for $CO_2$ and $H_2O$ in each studied surface. Unlike the $N_2$ adsorption, $H_2O$ was found to

**Table 3**
Calculated Vibrational Frequencies ($cm^{-1}$) for $CO_2$ molecule adsorption on $MoS_2$_1V$_S$, $MoS_2$_1V$_{Mo}$_1V$_S$ and $MoS_2$_1V$_{Mo}$_3N$_S$ sites. Calculated and Experimental values of gas-phase $CO_2$ molecule are included for comparison.

| Molecule | Gas-phase | | Physisorption on $MoS_2$_1V$_{Mo}$_1V$_S$/$MoS_2$_1V$_{Mo}$_3N$_S$ | | Dissociation on $MoS_2$_1V$_S$ |
|---|---|---|---|---|---|
| | Experimental | Theoretical | Current work | | |
| C═O | | | | | |
| stretching | 2349 [43,49] | 2360 [40] | 2361 | 2353/2355 | |
| Asymmetric ($\nu3$) | 1333 [43,49] | 1321 [40] | 1328 | 1315/1317 | |
| Symmetric ($\nu1$) | | | | | |
| C═O bending ($\nu2$) | 667 [43,49] | 638 [40] | 633 | 623/633 | |
| C≡O stretching | 2131 [43,49] | | | | 2119 |

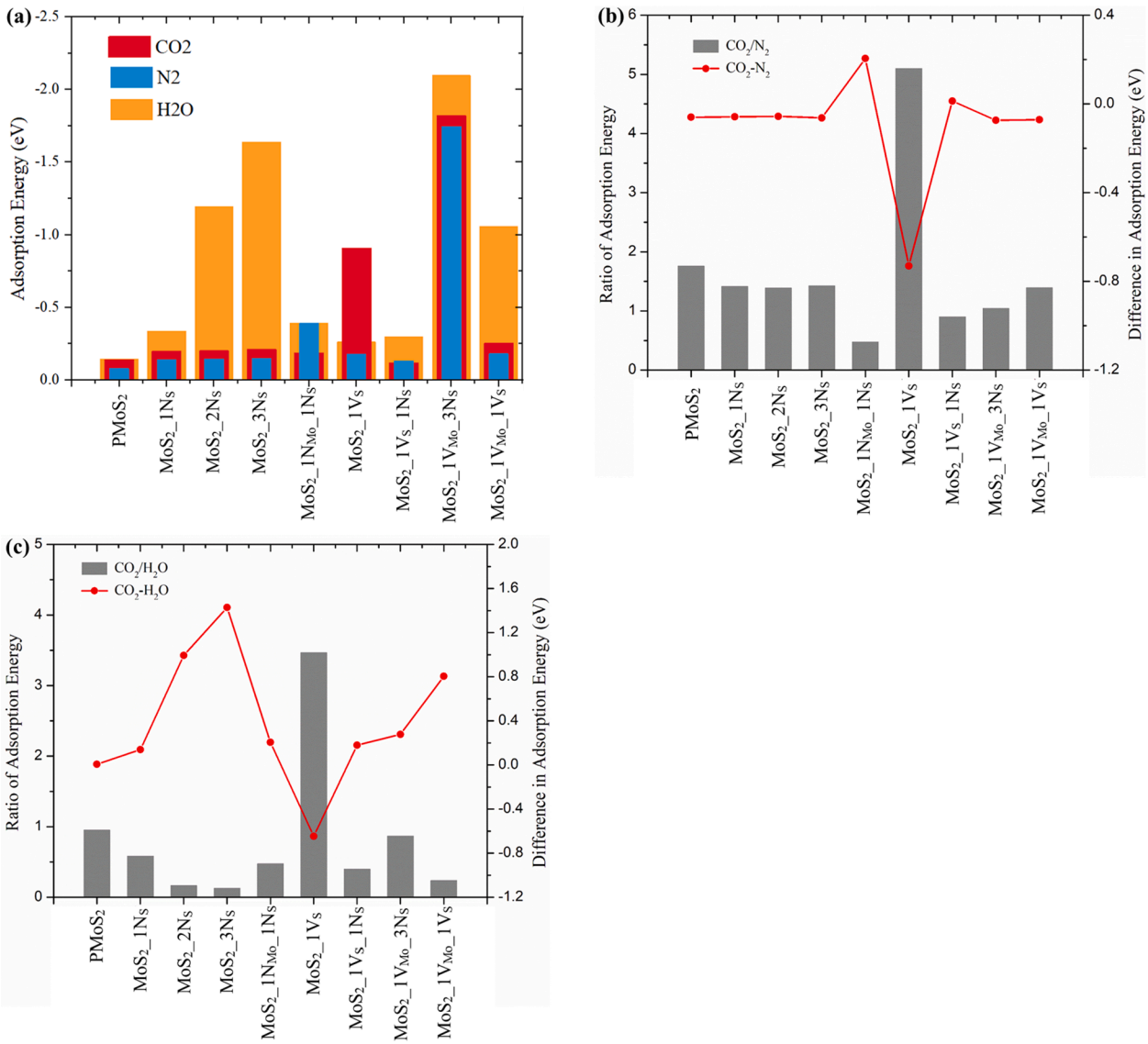


**Fig. 7.** Investigation of $CO_2$ adsorption selectivity over $N_2$ and the effect of moisture content (a) The adsorption energies of $CO_2$, $N_2$ and $H_2O$ molecules for the most stable adsorption configurations compared at 2.5 Å molecular height, (b) ratio and difference of adsorption energies between $CO_2$ and $N_2$ molecules, (c) ratio and difference of adsorption energies between $CO_2$ and $H_2O$ molecules.

bind more strongly on all the surfaces than $CO_2$ except on $MoS_2\_1V_S$ monolayer. The stronger adsorption of $H_2O$ molecule is characterized by its high polarity and quadrupole moment than those of $CO_2$. This is because the polarity of molecules adsorbed on any surface represents a very important factor that influences their interaction with the electric field of the surface. In other words, adsorbates that have the high quadrupole moment, such as $H_2O$, interact strongly with the electric field of $MoS_2$ monolayer and this favors their adsorption.

The highest ratio of 3.5 is obtained for $MoS_2\_1V_S$, whereas an adsorption ratio less than one is obtained for other surfaces. Also, by comparing the difference in adsorption energies for $CO_2$ and $H_2O$, it is evident that $MoS_2\_1V_S$ favors $CO_2$ adsorption over $H_2O$. The positive difference in the adsorption energies and low ratio of adsorption energies of $CO_2$ over $H_2O$ for the pristine, N-substitutional and double vacant systems indicate that the exhibit excellent selective adsorption of $H_2O$ over $CO_2$ molecule. Therefore, the presence of $H_2O$ could significantly decrease the adsorption capacity of these $MoS_2$ monolayer systems towards selective adsorption and separation of $CO_2$. Although the results showed that $MoS_2\_1V_S$ site is suitable adsorbent for selective adsorption and separation of $CO_2$, the optimization of the $MoS_2$ monolayers structural characteristics and the experimental conditions that will ensure the removal of water vapor to the lowest value might enhance substantially their $CO_2$ adsorption capacity and thereby might give rise to the excellent adsorbents that may be used to capturing the industrial emissions of $CO_2$. Finally, $CO_2$ appears to bind stronger on $MoS_2\_1V_{Mo}\_3N_S$ site than $N_2$, making it suitable adsorbent for selective adsorption and separation of $CO_2$ over $N_2$, but for the application of $CO_2$ storage, the existence of $H_2O$ may affect the partial charge distribution of the nitrogen doped vacancy sites.

## 4. Conclusions

It can be concluded that all of the considered surfaces with vacancy defects and N-doping at the vacancy site exhibit superior adsorption activity, selectivity and stability except for the N-substituted Mo atom ($MoS_2\_1N_{Mo}$) surface. Among the 10 different surface models studied, the 1 sulfur-vacancy ($MoS_2\_1V_S$) and tertiary nitrogen doped 1 Mo-vacancy ($MoS_2\_1V_{Mo}\_3N_S$) exhibit strong binding energies of −0.908 and −1.818 eV, respectively. These values are approximately 7 and 13 times as strong as that of a pristine $MoS_2$ surface. The results reveal that

$CO_2$ mainly adsorbs on the basal plane of pristine $MoS_2$ surface as a result of van der Waals interactions, while the vacancy defect and N doping perturb the local electron density of $MoS_2$ surfaces and greatly promote $CO_2$ adsorption with covalent and electrostatic interactions. Among various vacancy defects, $MoS_2\_1V_S$ improved adsorption efficiency of $CO_2$ through dissociative chemisorption, leading to reduction of $CO_2$ to CO gas. This phenomenon is promoted by the perpendicular orientation of the $CO_2$ molecule after geometric optimization, which increased the covalent attractions at the vacant site. Meanwhile, a double molybdenum and sulfur (MoS) vacancy defect ($MoS_2\_1V_{Mo}\_1V_S$) facilitates $CO_2$ physisorption by enhancing the van der Waals interactions between $CO_2$ and the basal plane of the vacancy site. The promotional effects of tertiary nitrogen doping of 1 Mo-vacancy on $CO_2$ physisorption can be attributed to the enhanced electrostatic interactions.

In addition, $MoS_2\_1V_S$ and $MoS_2\_1V_{Mo}\_3N_S$ surfaces showed a stronger selective adsorption of $CO_2$ over $N_2$. Due to stronger adsorption energy of $H_2O$ over $CO_2$ at the tertiary nitrogen doped 1 Mo-vacancy site, application of this material for $CO_2$ storage maybe limited by moisture, by affecting the partial charge distribution of the nitrogen species at the vacancy site. The results in this study are expected to be helpful to reveal the $CO_2$ adsorption mechanism and develop $CO_2$ adsorbents based on $MoS_2$ materials containing nitrogen. These will provide new insights for improved molecular adsorption on heteroatom-doped $MoS_2$ surfaces, which has been witnessed on carbon surfaces.

## Declaration of Competing Interest

The authors declare that they have no known competing financial interests or personal relationships that could have appeared to influence the work reported in this paper.

## Acknowledgement

This work was supported by the New Materials Institute (NMI), University of Nottingham Ningbo China (UNNC). The Zhejiang Provincial Department of Science and Technology is acknowledged for this research under its Provincial Key Laboratory Program (2020E10018). Ningbo Bureau of Science and Technology is thanked for sponsoring the Municipal Key Laboratory of Clean Energy Conversion Technologies; Ningbo Bureal of Education is appreciated for its funding to Municipal Comprehensive Collaborative Innovation Centre. We are also grateful for the access to the University of Nottingham High Performance Computing facility both in Ningbo China and Nottingham UK. Hainam Do is grateful for a research fund for International Young Scientists from the National Natural Science Foundation of China (Grant No. 21850410456). Special thanks to the Computational Chemistry Super Group (compchemsupergroup) of University of Nottingham United Kingdom. We thank Prof. Jonathan Hirst for his helpful discussions and insight on this work, and Linbin Yao for the graphical work. In addition, we thank Prof. Kieron Burke for his helpful insights on the issue of delocalization error found in PBE-GGA functional. Elena Besley acknowledges a Royal Society Wolfson Fellowship for financial support.

## Appendix A. Supplementary material

Supplementary data to this article can be found online at https://doi.org/10.1016/j.apsusc.2020.148556.

## References

[1] K. Lv, C. Teng, M. Shi, Y. Yuan, Y. Zhu, J. Wang, Z. Kong, X. Lu, Y. Zhu, Hydrophobic and electronic properties of the E-MoS2 nanosheets induced by FAS for the CO2 electroreduction to syngas with a wide range of CO/H2 ratios, Adv. Funct. Mater. 28 (2018) 1802339.
[2] S. Budinis, S. Krevor, N.M. Dowell, N. Brandon, A. Hawkes, An assessment of CCS costs, barriers and potential, Energy Strategy Rev. 22 (2018) 61–81.
[3] M. Chhowalla, H.S. Shin, G. Eda, L.-J. Li, K.P. Loh, H. Zhang, The chemistry of two-dimensional layered transition metal dichalcogenide nanosheets, Nat. Chem. 5 (2013) 263.
[4] X. Chia, A. Adriano, P. Lazar, Z. Sofer, J. Luxa, M. Pumera, Layered platinum dichalcogenides (PtS2, PtSe2, and PtTe2) electrocatalysis: monotonic dependence on the chalcogen size, Adv. Funct. Mater. 26 (2016) 4306–4318.
[5] A.S. Rad, First principles study of Al-doped graphene as nanostructure adsorbent for $NO_2$ and $N_2O$: DFT calculations, Appl. Surf. Sci. 357 (2015) 1217–1224.
[6] A.S. Rad, E. Abedini, Chemisorption of NO on Pt-decorated graphene as modified nanostructure media: a first principles study, Appl. Surf. Sci. 360 (2016) 1041–1046.
[7] A.S. Rad, O.R. Kashani, Adsorption of acetyl halide molecules on the surface of pristine and Al-doped graphene: ab initio study, Appl. Surf. Sci. 355 (2015) 233–241.
[8] A. Shokuhi Rad, D. Zareyee, M. Peyravi, M. Jahanshahi, Surface study of gallium- and aluminum- doped graphenes upon adsorption of cytosine: DFT calculations, Appl. Surf. Sci. 390 (2016) 444–451.
[9] A.S. Rad, S.S. Shabestari, S.A. Jafari, M.R. Zardoost, A. Mirabi, N-doped graphene as a nanostructure adsorbent for carbon monoxide: DFT calculations, Mol. Phys. 114 (2016) 1756–1762.
[10] S. Muhammad Hafiz, R. Ritikos, T.J. Whitcher, N.Md. Razib, D.C.S. Bien, N. Chanlek, H. Nakajima, T. Saisopa, P. Songsiriritthigul, N.M. Huang, S. A. Rahman, A practical carbon dioxide gas sensor using room-temperature hydrogen plasma reduced graphene oxide, Sens. Actuators, B 193 (2014) 692–700.
[11] V.P. Pham, G.Y. Yeom, Recent advances in doping of molybdenum disulfide: industrial applications and future prospects, Adv. Mater. 28 (2016) 9024–9059.
[12] K.F. Mak, C. Lee, J. Hone, J. Shan, T.F. Heinz, Atomically thin $MoS_2$: a new direct-gap semiconductor, Phys. Rev. Lett. 105 (2010), 136805.
[13] S. Zhao, J. Xue, W. Kang, Gas adsorption on MoS2 monolayer from first-principles calculations, Chem. Phys. Lett. 595–596 (2014) 35–42.
[14] A. Shokri, N. Salami, Gas sensor based on MoS2 monolayer, Sens. Actuators, B 236 (2016) 378–385.
[15] E.W. Keong Koh, C.H. Chiu, Y.K. Lim, Y.-W. Zhang, H. Pan, Hydrogen adsorption on and diffusion through MoS2 monolayer: First-principles study, Int. J. Hydrogen Energy 37 (2012) 14323–14328.
[16] S.-Y. Cho, S.J. Kim, Y. Lee, J.-S. Kim, W.-B. Jung, H.-W. Yoo, J. Kim, H.-T. Jung, Highly enhanced gas adsorption properties in vertically aligned $MoS_2$ layers, ACS Nano 9 (2015) 9314–9321.
[17] C. Ataca, S. Ciraci, Dissociation of $H_2O$ at the vacancies of single-layer $MoS_2$, Phys. Rev. B 85 (2012), 195410.
[18] D. Ma, W. Ju, T. Li, G. Yang, C. He, B. Ma, Y. Tang, Z. Lu, Z. Yang, Formaldehyde molecule adsorption on the doped monolayer $MoS_2$: a first-principles study, Appl. Surf. Sci. 371 (2016) 180–188.
[19] N. Yu, L. Wang, M. Li, X. Sun, T. Hou, Y. Li, Molybdenum disulfide as a highly efficient adsorbent for non-polar gases, Phys. Chem. Chem. Phys. 17 (2015) 11700–11704.
[20] J. Hong, Z. Hu, M. Probert, K. Li, D. Lv, X. Yang, L. Gu, N. Mao, Q. Feng, L. Xie, J. Zhang, D. Wu, Z. Zhang, C. Jin, W. Ji, X. Zhang, J. Yuan, Z. Zhang, Exploring atomic defects in molybdenum disulphide monolayers, Nat. Commun. 6 (2015) 6293.
[21] H. Li, M. Huang, G. Cao, Markedly different adsorption behaviors of gas molecules on defective monolayer $MoS_2$: a first-principles study, Phys. Chem. Chem. Phys. 18 (2016) 15110–15117.
[22] H. Schweiger, P. Raybaud, G. Kresse, H. Toulhoat, Shape and edge sites modifications of $MoS_2$ catalytic nanoparticles induced by working conditions: a theoretical study, J. Catal. 207 (2002) 76–87.
[23] O.G. Sánchez, Y.Y. Birdja, M. Bulut, J. Vaes, T. Breugelmans, D. Pant, Recent advances in industrial $CO_2$ electroreduction, Curr. Opin. Green Sustain. Chem. 16 (2019) 47–56.
[24] H. Wang, Z. Cheng, Y. Liao, J. Li, J. Weber, A. Thomas, C.F.J. Faul, Conjugated microporous polycarbazole networks as precursors for nitrogen-enriched microporous carbons for $CO_2$ storage and electrochemical capacitors, Chem. Mater. 29 (2017) 4885–4893.
[25] H. Li, J. Li, A. Thomas, Y. Liao, Ultra-high surface area nitrogen-doped carbon aerogels derived from a schiff-base porous organic polymer aerogel for $CO_2$ storage and supercapacitors, Adv. Funct. Mater. 29 (2019) 1904785.
[26] Shijun Zhao, Jianming Xue, W. Kang, Gas adsorption on $MoS_2$ monolayer from first-principles calculations, Chem. Phys. Lett. 595–596 (2014) 35–42.
[27] Q. Yue, Z. Shao, S. Chang, J. Li, Adsorption of gas molecules on monolayer $MoS_2$ and effect of applied electric field, Nanoscale Res. Lett. 8 (2013) 1–7.
[28] Y. Wang, S. Li, J. Yi, Electronic and magnetic properties of Co doped $MoS_2$ monolayer, Sci. Rep. 6 (2016) 24153.
[29] C. Ataca, S. Ciraci, Functionalization of single-layer $MoS_2$ honeycomb structures, J. Phys. Chem. C 115 (2011) 13303–13311.
[30] S. Grimme, Semiempirical GGA-type density functional constructed with a long-range dispersion correction, J. Comput. Chem. 27 (2006) 1787–1799.
[31] G. Kresse, J. Furthmüller, Efficient iterative schemes for ab initio total-energy calculations using a plane-wave basis set, Phys. Rev. B 54 (1996) 11169–11186.
[32] G. Kresse, J. Furthmüller, Efficiency of ab-initio total energy calculations for metals and semiconductors using a plane-wave basis set, Comput. Mater. Sci. 6 (1996) 15–50.
[33] S.E. Mason, P.H. Beton, N.A. Besley, AIRBED: A simplified density functional theory model for physisorption on surfaces, J. Chem. Theory Comput. 15 (2019) 5628–5634.
[34] J.P. Perdew, K. Burke, M. Ernzerhof, Generalized gradient approximation made simple, Phys. Rev. Lett. 77 (1996) 3865–3868.

[35] H.J. Monkhorst, J.D. Pack, Special points for Brillouin-zone integrations, Phys. Rev. B 13 (1976) 5188–5192.
[36] G. Henkelman, A. Arnaldsson, H. Jónsson, A fast and robust algorithm for Bader decomposition of charge density, Comput. Mater. Sci. 36 (2006) 354–360.
[37] N.A. Besley, J.A. Bryan, Partial hessian vibrational analysis of organic molecules adsorbed on Si(100), J. Phys. Chem. C 112 (2008) 4308–4314.
[38] P. Joensen, E.D. Crozier, N. Alberding, R.F. Frindt, A study of single-layer and restacked $MoS_2$ by X-ray diffraction and X-ray absorption spectroscopy, J. Phys. C: Solid State Phys. 20 (1987) 4043.
[39] F.M. Enujekwu, C.I. Ezeh, M.W. George, M. Xu, H. Do, Y. Zhang, H. Zhao, T. Wu, A comparative study of mechanisms of the adsorption of $CO_2$ confined within graphene–$MoS_2$ nanosheets: a DFT trend study, Nanoscale Adv. 1 (2019) 1442–1451.
[40] Y. Liu, J. Wilcox, $CO_2$ adsorption on carbon models of organic constituents of gas shale and coal, Environ. Sci. Technol. 45 (2011) 809–814.
[41] A.L. Allred, Electronegativity values from thermochemical data, J. Inorg. Nucl. Chem. 17 (1961) 215–221.
[42] A. Azcatl, X. Qin, A. Prakash, C. Zhang, L. Cheng, Q. Wang, N. Lu, M.J. Kim, J. Kim, K. Cho, R. Addou, C.L. Hinkle, J. Appenzeller, R.M. Wallace, Covalent nitrogen doping and compressive strain in $MoS_2$ by remote N2Plasma exposure, Nano Lett. 16 (2016) 5437–5443.
[43] CRC, Crc Handbook of Chemistry and Physics, 90th ed.;, CRC Press, Boca Raton, FL, 2009–2010..
[44] D. Saha, Z. Bao, F. Jia, S. Deng, Adsorption of $CO_2$, $CH_4$, $N_2O$, and $N_2$ on MOF-5, MOF-177, and Zeolite 5A, Environ. Sci. Technol. 44 (2010) 1820–1826.
[45] Y. Zheng, S. Zheng, H. Xue, H. Pang, Metal-organic frameworks/graphene-based materials: preparations and applications, Adv. Funct. Mater. 28 (2018) 1804950.
[46] A.A. Kistanov, S.K. Khadiullin, S.V. Dmitriev, E.A. Korznikova, Effect of oxygen doping on the stability and band structure of borophene nanoribbons, Chem. Phys. Lett. 728 (2019) 53–56.
[47] D. Ma, Q. Wang, T. Li, C. He, B. Ma, Y. Tang, Z. Lu, Z. Yang, Repairing sulfur vacancies in the $MoS_2$ monolayer by using CO, NO and $NO_2$ molecules, J. Mater. Chem. C 4 (2016) 7093–7101.
[48] J. Li, M. Hou, Y. Chen, W. Cen, Y. Chu, S. Yin, Enhanced $CO_2$ capture on graphene via N, S dual-doping, Appl. Surf. Sci. 399 (2017) 420–425.
[49] W.B. Person, G. Zerbi, Vibrational intensities in infrared and Raman spectroscopy, Amsterdam : Elsevier scientific, 1982.
[50] D.S. Sholl, J.A. Steckel, Accuracy and Methods beyond “Standard” Calculations, Density Functional Theory: A Practical Introduction, John Wiley & Sons Inc, Hoboken, NJ, 2009, pp. 209–233.